

Electric-field-tuned binding energies of trions in silicene, germanene, and stanene monolayers

Roman Ya. Kezerashvili^{1,2}, Shalva M. Tsiklauri,³ and Anastasia Spiridonova¹

¹*New York City College of Technology, The City University of New York, USA*

²*The Graduate School and University Center, The City University of New York, USA*

³*Borough of Manhattan Community College, The City University of New York, USA*

(Dated: May 31, 2024)

We predict a formation of intravalley and intervalley controllable trions in buckled 2D materials such as silicene, germanene and stanene monolayers in an external electric field. A study is performed within the framework of a nonrelativistic potential model using the method of hyperspherical harmonics (HH). We solve the three-body Schrödinger equation with the Rytova-Keldysh potential by expanding the wave functions of a trion in terms of the HH. A resultant system of coupled differential equations are solved numerically. Controllable ground state energies of intravalley and intervalley trions by the external electric field are presented. The dependencies of the binding energy (BE) of trions in the silicene, germanene and stanene as a function of the electric field are qualitatively similar. BEs of trions formed by *A* and *B* excitons have a non-negligible differences which slightly increase as the electric field increases. It is demonstrated that trion BEs can be controlled by the external electric field and the dielectric environment has a significant effect on the trion BE.

I. INTRODUCTION

The prediction of the existence of trions [1] consisting from an exciton and electron or hole known as negatively or positively charged excitons (X^\mp) gave rise to many theoretical and experimental studies of trions in bulk materials, quantum-well systems, and two-dimensional (2D) materials. Atomically thin transition metal dichalcogenides (TMDCs) are a class of two-dimensional (2D) materials with remarkable optical and electronic properties [2, 3]. Since 2013, when trions were observed in two-dimensional MoS_2 monolayers [4], trions are the subject of intense studies, both experimentally and theoretically in monolayer transition metal dichalcogenides (TMDCs). In the past decade, different experimental groups observed and reported the signature of a trion in TMDCs monolayers.

Theoretical studies of trions have integrated a wide variety of techniques and carried out to calculate the binding energies (BEs) of excitonic complexes in monolayer TMDCs (see reviews [5–9]). The first calculations of the BEs of trions in TMDC was performed using the variational method and then different approaches were used in calculations such as the stochastic variational method with correlated Gaussian basis, the diffusion quantum Monte Carlo and path-integral Monte Carlo methods, a direct diagonalization of the three-particle Hamiltonian within the Tamm–Dancoff approximation, the finite element method, the hyperspherical harmonic method and three-body Faddeev equations in configuration or momentum spaces which we are citing in a chronological order [10–38]. Results for BEs of trions in TMDC monolayers yielded impressively accurate results consistent with experimental data.

Another category of 2D semiconductors are the buckled 2D allotropes of silicon, germanium, and tin, known as silicene, germanene, and stanene, and collectively referred to as Xenes [39, 40]. Experimental studies revealed one of the most crucial differences between Xenes and graphene and TMDC that Xenes monolayer is not a perfectly flat sheet, but instead is slightly buckled [39, 41]. As a result, this unique structure of Xenes makes them sensitive to the external electric field applied perpendicular to the monolayer allowing to open and control the band gap. The tunable band gap of Xenes gives researchers, among other things, extraordinary in situ control over binding energies and optical properties of excitons in these materials.

In contrast to TMDCs, there is no extensive research on excitonic complexes in Xenes monolayers. The reason is that the synthesis of Xenes monolayers has not been as successful and extensive, as for example, TMDCs monolayers because Xenes monolayers are unstable in the air [42, 43]. In contrast to graphene, silicene and other Xenes monolayers do not occur in nature. Nevertheless, silicene nanoribbons were experimentally synthesized on a metal substrate [44, 45]. This opened the way for silicene, germanene, and stanene monolayers being transferred on metal like Au [46–50] and substrates such as MoS_2 , Ir, ZrB_2 [49, 51] and hexagonal boron nitride (hBN) [52, 53] and synthesized as freestanding monolayers [54]. Working with a metallic substrate is easier. For example, silicene grown on Ag (111) [43, 55] and germanene synthesized by dry deposition on Au (111) surface [48] have been thoroughly investigated. However, depositing Xene on a metal leads to a significant alteration of properties of the Xene monolayer. Depending on a substrate, properties of Xenes monolayers vary, see Refs. [39, 52] for the list of Xenes properties on different substrates. In opposition to deposition on a metal, depositing Xenes on hBN is harder. However, Xene deposited on hBN preserves its properties because Xene and hBN weakly interact [52]. Xenes monolayers deposited on hBN present a particular interest for studying magnetoexcitons in monolayer and vdWHs [56].

Xenes optical and magneto-optical properties have been addressed in Refs. [41, 57–59] and [60, 61], respectively. Different physical phenomena, such as the Hall effect [55], the valley-locked spin-dependent Seebeck effect [62], anomalous quantum Hall effect [63], quantum spin Hall effect [64], and the Landau levels [55, 60, 65] are studied because of their essential role in applications of Xenes monolayers in nano- and quantum devices [64, 66–69].

Because of the band inversion, these honeycomb materials are also topological insulators [70–75]. The existence of an excitonic insulator phase in silicene, germanene and stanene have been first studied by Brunetti et al. [76, 77] in the framework of the effective mass approximation. The influence of the screening, band dispersion and external electric field on transitions in Xenes between excitonic, topological, and trivial insulator phases were investigated in [78].

Currently, there is a shortage of research on exciton complexes in Xenes. In particular, a study of the formation of three quasiparticle states, trions, in Xenes monolayers. In this paper, we address this gap and focus on a theoretical investigation of trions in Xenes within the method of hyperspherical harmonics (HH).

The paper is organized as follows. In Sec. II, we present the theoretical model and formalism to study Mott-Wannier trions in Xenes within the framework of the method of hyperspherical harmonics. We consider a nonrelativistic potential model for three interacting electrons and holes system and employ the three-body Schrödinger equation in the effective mass approximation. In the framework of the HH method, the Schrödinger equation with the Rytova-Keldysh potential [79, 80] is reduced to the system of coupled differential equations for the hyperradial functions. A numerical solution of this system provides the BE and wavefunction for trions in Xenes. In Sec. III, we discuss a classification of intravalley and intervalley trions in Xenes monolayers (Subsec. III A) and present results of calculations of controllable ground state energies of intravalley and intervalley trions by the external electric field (Subsec. III B). Here we analyze the dependencies of the BEs and probability distributions of three bound particles on the external electric field. Based on the capability to control a BE and compactness of trions in Xenes by the external electric field, we discuss a proposal of a possible trions crystallization in Xenes and estimate corresponding densities of composite fermions gas. Conclusions follow in Sec. IV.

II. THEORETICAL MODEL

We start by providing the framework of the low-energy model describing exciton states in Xenes monolayers and heterostructures when the external electric field perpendicular to a monolayer is present. Silicene, germanene, and stanene monolayers are 2D buckled materials and have honeycomb structure like graphene. However, in contrast to graphene, the most stable form of Si, Ge, and Sn monolayers is honeycomb lattice with the offset of triangular sublattices A and B with respect to the monolayer's plane. The offset is denoted by d_0 and known as the buckling constant or buckling factor. As a result of the buckled structure of Xenes monolayers, they are sensitive to the external electric field applied perpendicular to a monolayer. This manifests as an on-site potential difference between sublattices when the electric field is applied. When the external electric field is not applied, the band structure of Xenes monolayers in the vicinity of the K/K' points resembles graphene band structure. However, the intrinsic gaps of Xenes are larger than the band gaps in graphene. The application of the external electric field perpendicular to the monolayer leads to a potential difference between sublattices A and B that changes the band gap resulting in changes in the effective masses of the electrons and holes.

The single-particle spectrum of electronic states in monolayer Xenes in the electric field acting along the z -axis in the vicinity of the K/K' points reads ($\hbar = c = 1$) [81]:

$$\hat{H} = v_F (\xi p_x \hat{\tau}_x + p_y \hat{\tau}_y) - \xi \Delta_{gap} \hat{\sigma}_z \hat{\tau}_z + \Delta_z \hat{\tau}_z. \quad (1)$$

In Eq. (1) v_F is the Fermi velocity, $\xi, \sigma = \pm 1$ are the valley and spin indices, respectively, p_x and p_y are the components of momentum in the xy -plane of the monolayer relative to the K point, $\hat{\tau}$ and $\hat{\sigma}$ are the pseudospin and real spin Pauli matrices, respectively, $2\Delta_{gap}$ is the intrinsic band gap, and $\Delta_z = ed_0 E_\perp$ is the gap induced by the electric field, E_\perp , acting along the z -axis. The first term in Hamiltonian (1) is the same as that of the low-energy Hamiltonian in graphene [82, 83], the second term is the spin-orbit coupling with an intrinsic band gap of $2\Delta_{gap}$, the last term describes the sublattice potential difference appearing when the external electric field is applied [46, 47, 84, 85].

From Eq. (1), the low-energy eigenvalues for charge carriers near the K/K' points can be written as [81]:

$$E(k) = \sqrt{\Delta_{\xi\sigma}^2 + v_F^2 p^2}, \quad (2)$$

where

$$\Delta_{\xi\sigma} = |\xi\sigma\Delta_{gap} - ed_0 E_\perp| \quad (3)$$

is the electric-field-dependent band gap at $p = 0$. When there is no external electric field, the spin-up and spin-down bands of the valence and conduction bands are degenerate. Application of E_\perp lifts this degeneracy by splitting both the valence and conduction bands. When $\xi = -\sigma$, the gap is large, since conduction and valence bands are the furthest from the Fermi energy level, and the electron and hole form A excitons. When $\xi = \sigma$, the gap is small, since conduction and valence bands are the closest, and the electron and hole form B exciton. To open the band gap $\Delta_{\xi\sigma}$, a critical value of the electric field has to be achieved $E_c = \Delta_{gap}/(ed_0)$ and then the lower bands form a Dirac cone at K/K' points. The critical values of the electric field for Xenes monolayers are given in Ref. [77]. Parabolic conduction and valence bands in the vicinity of K/K' points allow to find the effective mass of charge carriers as $m = \Delta_{\xi\sigma}/v_F^2$. In Xenes monolayers the lowest conduction and the highest valence bands are symmetric, therefore, the effective masses of an electron and hole are the same and can be written as a function of the external electric field:

$$m = \frac{|\xi\sigma\Delta_{gap} - ed_0E_\perp|}{v_F^2}. \quad (4)$$

Analyses of Eq. (4) shows that the value of the electron or hole effective mass depends on the band gap, Fermi velocity, buckling constant and is a function of E_\perp .

A. Effective mass approach for trions in buckled 2D materials

The promotion of an electron from the filled valence band to the empty conduction band leaves an empty electron state in the valence band. The description of such many-body system can be reduced to the two-particle problem of the negatively charged conduction electron interacting with a positively charged valence hole that form an exciton or other excitonic complexes such as charged excitons or trions. The trions are formed when an exciton binds another electron or hole to form a negatively or positively charged three-particle system: X^- or X^+ , respectively. A description of properties of trions requires a solution of a three-particle problem. In buckled two-dimensional monolayers, the resulting trions we consider as the Wannier-Mott trions since the correlation between an electron and a hole extends over many lattice periods. The representation of the electron-hole pair bound in a Wannier-Mott exciton shows the strong spatial correlation of these two constituents. Therefore, we are assuming that the interaction of the exciton with the third particle (electron or hole) leads to a large-radius type system.

We follow the approach in which one assumes that the electron and hole bands are isotropic and parabolic, which is a good approximation for the low-energy spectrum of 2D materials. This form of the Hamiltonian implies that both the electron and hole single particle states form a single parabolic band. The corresponding eigenproblem equation reduces to the Schrödinger equation in the effective mass approximation. This approach is common in the literature to describe excitons and trions in 2D materials. See, for example, Refs. [2, 6, 8, 38, 86–90]. Below, we follow the effective mass approximation.

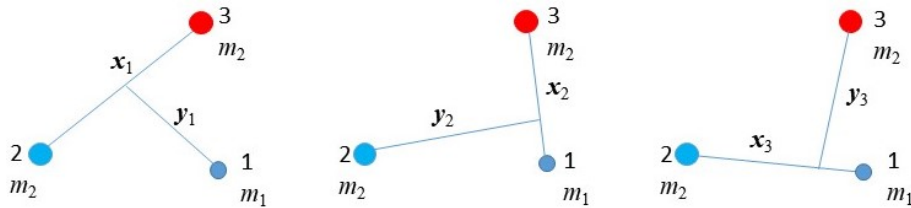


FIG. 1: (Color online) Schematics of partition trees of Jacobi coordinates when two particles have the same masses. The electron and hole in one electron-hole pair have the same masses. This corresponds to the intravalley X^- and X^+ trions.

In order to obtain the eigenfunctions and eigenenergies of a 2D trion in Xenes when the electric field is perpendicular to the Xenes monolayer, we write the Schrödinger equation for an interacting three-particle electron-hole system. Because we are considering the varying electric field E_\perp , which is directed along z -axis, the corresponding term in the 2D Schrödinger equation vanishes. However, the effect of the electric field action is present through the effective mass as follows from Eq. (4). Thus, one can write 2D Schrödinger equation for the interacting three-particle electron-hole system within the effective mass approximation in the following form

$$\left[-\frac{\hbar^2}{2} \sum_{i=1}^3 \frac{1}{m_i} \nabla_i^2 + \sum_{i < j}^3 V_{ij}(|\mathbf{r}_i - \mathbf{r}_j|) \right] \Psi(\mathbf{r}_1, \mathbf{r}_2, \mathbf{r}_3) = E\Psi(\mathbf{r}_1, \mathbf{r}_2, \mathbf{r}_3), \quad (5)$$

where m_i is the effective mass of the electron or hole defined by Eq. (4) and \mathbf{r}_i is the i th particle position. We assume only two types of charge carriers: electron and hole with the corresponding effective masses. In Eq. (5), $V_{ij}(|\mathbf{r}_i - \mathbf{r}_j|)$ is the interaction potential between q_i and q_j charges in a 2D material that was first derived in Ref. [79] and was independently obtained by Keldysh [80]. We refer to it as the Rytova-Keldysh (RK) potential. The Rytova-Keldysh potential describes the Coulomb interaction screened by the polarization of the electron orbitals in the 2D lattice and has the following form

$$V_{ij}(r) = \frac{\pi k q_i q_j}{2\kappa \rho_0} \left[H_0\left(\frac{r}{\rho_0}\right) - Y_0\left(\frac{r}{\rho_0}\right) \right], \quad (6)$$

where $r = |\mathbf{r}_i - \mathbf{r}_j|$ is the relative coordinate between two charge carriers q_i and q_j . In Eq. (6) $k = 9 \times 10^9 \text{ N}\cdot\text{m}^2/\text{C}^2$, κ is the dielectric constant of the environment that is defined as $\kappa = (\varepsilon_1 + \varepsilon_2)/2$, where ε_1 and ε_2 are the dielectric constants of two materials that the Xenon layer is surrounded by, ρ_0 is the screening length, which sets the boundary between two different behaviors of the potential due to a nonlocal macroscopic screening, and $H_0(\frac{r}{\rho_0})$ and $Y_0(\frac{r}{\rho_0})$ are the Struve function and Bessel function of the second kind, respectively. The screening length ρ_0 can be written as $\rho_0 = (2\pi\chi_{2D})/(\kappa)$ [86], where χ_{2D} is the 2D polarizability, which in turn is given by $\chi_{2D} = l\varepsilon/4\pi$ [80], where ε is the bulk dielectric constant of the Xenon monolayer. For large distances $r \gg \rho_0$ the potential has the three-dimensional bare Coulomb tail $V_{ij}(r) = \frac{kq_i q_j}{\varepsilon r}$, while at very small distances, smaller than the screening length $r \ll \rho_0$, it becomes a logarithmic potential like a potential of a point charge in two dimensions: $V_{ij}(r) = \frac{kq_i q_j}{\varepsilon \rho_0} \left[\ln\left(\frac{r}{2\rho_0}\right) + \gamma \right]$, where γ is the Euler constant. Therefore, the potential (6) becomes the standard bare Coulomb potential at $r \gg \rho_0$ and diverges logarithmically at $r \ll \rho_0$. A crossover between these two regimes takes place around distance ρ_0 . Thus, at small distances between charge carriers the short-range interaction strength decreases, while the long-range interaction strength is unaffected and is the bare three-dimensional Coulomb potential. It is worth noting that in Ref. [91] a very good approximation to the RK potential that is simpler to use, fairly precise in both limits and remarkably accurate for all distances was introduced.

To obtain a solution of the Schrödinger equation (5) for the negatively and positively charged trions, we use the method of hyperspherical harmonics (HH) [92]. The main idea of this method is the expansion of the wave function of the trion in terms of HH that are the eigenfunctions of the angular part of the Laplace operator in the four-dimensional (4D) space. As the first step, let us separate the center-of-mass (c.m.) and the relative motion of three particles and introduce sets of mass-scaled Jacobi coordinates [92, 93]. There are three equivalent sets of Jacobi coordinates and there is the orthogonal transformation between these sets [94, 95]. For three non identical particles that have different masses the mass-scaled Jacobi coordinates for the partition i read as follows [92–94]:

$$\begin{aligned} \mathbf{x}_i &= \sqrt{\frac{m_j m_k}{(m_j + m_k)\mu}} (\mathbf{r}_j - \mathbf{r}_k), \\ \mathbf{y}_i &= \sqrt{\frac{m_i (m_j + m_k)}{(m_i + m_j + m_k)\mu}} \left(\frac{m_j \mathbf{r}_j + m_k \mathbf{r}_k}{m_j + m_k} - \mathbf{r}_i \right), \quad i \neq j \neq k = 1, 2, 3, \end{aligned} \quad (7)$$

where

$$\mu = \sqrt{\frac{m_i m_j m_k}{m_i + m_j + m_k}} \quad (8)$$

is the three-particle effective mass. In Eqs. (7) the subscripts i , j , and k are a cyclic permutation of the particle numbers. Trees of Jacobi coordinates for a three-particle system, when two particles have the same masses, are shown in Fig. 1.

The transformation (7) allows the separation of c.m. and relative motions of three particles with Hamiltonian (5), and the Schrödinger equation for the relative motion of the three-body system reads

$$\left[-\frac{\hbar^2}{2\mu} (\nabla_{\mathbf{x}_i}^2 + \nabla_{\mathbf{y}_i}^2) + V(x_1) + V(x_2) + V(x_3) \right] \Psi(\mathbf{x}_i, \mathbf{y}_i) = E \Psi(\mathbf{x}_i, \mathbf{y}_i). \quad (9)$$

In Eq. (9), $V(x_i)$ is the interaction potential between two particles at the relative distance x_1 , x_2 , and x_3 , respectively, where x_i is the modulus of the Jacobi vector \mathbf{x}_i (7), and (9) is written for any of set $i = 1, 2, 3$ of the Jacobi coordinates (7). The orthogonal transformation between three equivalent sets of the Jacobi coordinates simplifies calculations of matrix elements involving $V(x_i)$ potentials.

This method is presented in detail in Ref. [38] and is briefly outlined here. We introduce in the 4D space the hyperradius $\rho = \sqrt{x_i^2 + y_i^2}$ and a set of three angles $\Omega_i \equiv (\alpha_i, \varphi_{x_i}, \varphi_{y_i})$, where φ_{x_i} and φ_{y_i} are the polar angles for the Jacobi vectors \mathbf{x}_i and \mathbf{y}_j , respectively, and α_i is an angle defined as $x_i = \rho \cos \alpha_i$, $y_i = \rho \sin \alpha_i$. Next, we rewrite the Schrödinger equation (9) for the trion using hyperspherical coordinates in the 4D configuration space [38]. This transformation allows to reduce the solution of the problem for the three particles in the 2D configuration space to the motion of one particle in the 4D configuration space. Then we introduce the hyperspherical harmonics $\Phi_{K\lambda}(\Omega)$ in the 4D configuration space, which are the eigenfunctions of the angular part of the generalized Laplace operator $\hat{K}^2(\Omega_i)$ in the 4D configuration space $\hat{K}^2(\Omega_i)\Phi_{K\lambda}(\Omega) = K(K+2)\Phi_{K\lambda}(\Omega)$ [92], where K is a grand angular momentum. Here we are using the short-hand notation $\lambda \equiv \{l_x, l_y, L, M\}$, where L is the total orbital angular momentum of the trion, M is its projection, and the grand angular momentum $K = 2n + l_x + l_y$, l_x , where l_y are angular momentum corresponding to \mathbf{x} and \mathbf{y} Jacobi coordinates, respectively, and $n \geq 0$ is an integer number.

The functions $\Phi_{K\lambda}(\Omega)$ present a complete set of orthonormal basis, and one can expand the wave function of the trion $\Psi(\rho, \Omega_i)$ in terms of the HH $\Phi_{K\lambda}(\Omega)$ as

$$\Psi(\rho, \Omega_i) = \rho^{-3/2} \sum_{K\lambda} u_{K\lambda}(\rho) \Phi_{K\lambda}(\Omega_i). \quad (10)$$

In Eq. (10) $u_{K\lambda}(\rho)$ are the hyperradial functions and by substituting (10) into the Schrödinger equation written in the hyperspherical coordinated [38], one can separate the radial and angular variables and get a set of coupled differential equations for the hyperradial functions $u_{K\lambda}(\rho)$:

$$\left[\frac{d^2}{d\rho^2} - \frac{(K+1)^2 - 1/4}{\rho^2} + \kappa^2 \right] u_{K\lambda}(\rho) = \frac{2\mu}{\hbar^2} \sum_{K'\lambda'} \mathcal{W}_{K\lambda K'\lambda'}(\rho) u_{K'\lambda'}(\rho). \quad (11)$$

In Eq. (11) $\kappa^2 = 2mB/\hbar^2$, where B is trion BE. The coupling effective potential energy $\mathcal{W}_{K\lambda K'\lambda'}(\rho)$ is

$$\mathcal{W}_{K\lambda K'\lambda'}(\rho) = \int \Phi_{K\lambda}^*(\Omega_i) \sum_{i < j}^3 V_{ij}(|\mathbf{r}_i - \mathbf{r}_j|) \Phi_{K'\lambda'}(\Omega_i) d\Omega_i. \quad (12)$$

The coupling effective interaction (12) is defined via the RK potential (6). Substituting (6) into Eq. (12), one obtains the matrix elements of the effective potential energies. The method of calculations of the effective potential energies is given in [38]. Calculations of matrix elements $\mathcal{W}_{K\lambda K'\lambda'}(\rho)$ of the two-body $V_{ij}(|\mathbf{r}_i - \mathbf{r}_j|)$ interactions in the hyperspherical harmonics expansion method for a three-body system is greatly simplified by using the HH basis states appropriate for the partition corresponding to the interacting pair. Using the matrix elements $\mathcal{W}_{K\lambda K'\lambda'}(\rho)$ in Eq. (11), one can solve the system of coupled differential equations numerically. Results of numerical solutions of (12) for trions in Xenes are presented in the next section.

III. TRIONS IN XENES

We apply the present theoretical approach for calculations of the trion BEs in the following Xenes monolayers: silicene (Si), germanene (Ge), and stanene (Sn). A schematic representation of a trion in freestanding, supported, and encapsulated Xenes monolayers in the external electric field $E_z = E_\perp$ perpendicular to the Xene layer is given in Fig. 2. The form of the trion wave function (10) is the most general, not restricted to any particular mass ratio of electrons and holes, and describes the three-particle relative motion. The splitting of the conduction and valence bands in Xenes due to spin-orbit coupling at non-zero electric fields leads to the formation of A and B excitons in the larger or smaller band gaps, with corresponding larger or smaller masses of the electron and hole. Two of the three particles constituting a positive or a negative trion in the Xene monolayer have the same masses due to the equity of the mass of electron and hole that form an exciton. However, they are not identical because they have different charges. An intervalley trion may have the same masses of three particles but they are not identical due to the different spin and/or valley indices. Below we consider trions formed by a singlet bright A or B exciton and an electron (X^-) or hole (X^+). Trion can be in either a single or triplet state.

A. Intravalley and intervalley trions

In 2D monolayer of Xenes intravalley and intervalley trions can be formed. Let us first consider intravalley trions. An interaction of bright the A or B exciton with another charged carrier in the same valley, which can either be an

electron or a hole, forms X^- or X^+ intravalley trion. Schematics in Fig. 3 show the possible formations of the X^- (Figs. 3a and 3b) and X^+ (Figs. 3c and 3d). As follows from Eq. (4), the electron and hole effective masses in A exciton are the same. The B excitons are composed of electron and hole which also have equal masses but smaller than masses of the electron and hole in A excitons. We denoted these masses as m_A and m_B , respectively. The intravalley X^- and X^+ trions have the same two particles masses. As follows from Eq. (8), the effective masses of the X^- and X^+ trions formed by A or B exciton are $\mu_A = \sqrt{\frac{m_B m_A^2}{m_B + 2m_A}}$ and $\mu_B = \sqrt{\frac{m_A m_B^2}{m_A + 2m_B}}$, respectively [38]. Because $m_A > m_B$, it follows that $\mu_A > \mu_B$. Therefore, the effective mass of the X^- and X^+ trions formed by the A exciton is larger than mass of the X^- and X^+ trions formed by the B exciton. Due to the proportionality of the BE of trions to the three-particle effective mass μ [38], a BE of X^- and X^+ trions formed by the A exciton is larger than BE of trions formed by the B exciton. In the ground state, both intravalley trions formed by charge carriers from the same valley are spin-singlet trions.

Intervalley X^- trions result from the attraction between K valley bright A excitons with an electron from K' valley or bright B excitons from the K valley with an electron from the K' valley. The effective masses of the X^- intervalley trions formed by bright A excitons is always larger than the effective masses of trions formed by B excitons. The corresponding spin-valley configurations are presented in Figs. 3e, 3f, 3g, and 3h. We should mention that the intervalley X^+ trions have the same masses as the X^- trions formed by the K valley bright A and B excitons due to the interaction with a hole from the K' valley. While intravalley trions are composed two particle with the same masses, intervalley trions can be a system of three particles with the same masses (Figs. 3e and 3h) or a three-particle system with two particles that have the same masses (Figs. 3f and 3g).

B. Results of calculations

The intravalley X^- and X^+ trions in Xenes monolayers have two particles (the electron and hole) that have the same masses and the third particle (the electron or hole) has a different mass as seen in Figs. 3a – 3d. Therefore, we have to deal with three non-identical particles because two particles with the same masses have different charges. For intervalley trions we have two cases: X^- and X^+ trions formed by the electron and hole with the same masses and the third particle has a different mass (spin-valley configurations in Figs. 3f and 3g) or all three particles have the same masses (spin-valley configurations in Figs. 3e and 3h). In the latter case, while three particles have the same masses, two belong to different valleys.

In calculations of the BEs of trions in Xenes monolayers, we use the RK potential. We solve the system of coupled differential equations (11) for the hyperradial functions $u_{K\lambda}^L(\rho)$ numerically. By solving the system of equations (11), one finds the binding energy as well as the corresponding hyperradial functions. The latter allows one to construct the wave function (10). Numerical solution of the coupled differential equations requires the control of the convergence of the BEs for trions with respect to the grand angular momentum K for each value of the external electric field. The relative convergence of the BE is checked as $\Delta B/B = [B(K+2) - B(K)]/B(K)$, where $B(K)$ is the BE for the given K . The analysis of the results for the BEs at different values of the electric field shows that the reasonable convergence is reached for $K_{\max} = 12$, so we limit our considerations to this value.

We considered the formation of trions in the singlet and triplet ground states and computed the corresponding BEs. The input parameters for calculations of BEs of trions in the freestanding, supported on SiO_2 and hBN encapsulated Xene monolayers are presented in Table I. The formation of Wannier–Mott excitons due to the electron-hole interaction via the RK potential in semiconducting phases in Xenes monolayers occurs when the external electric field exceed some critical value which is unique to each material [76]. A value of the critical electric field is slightly different for

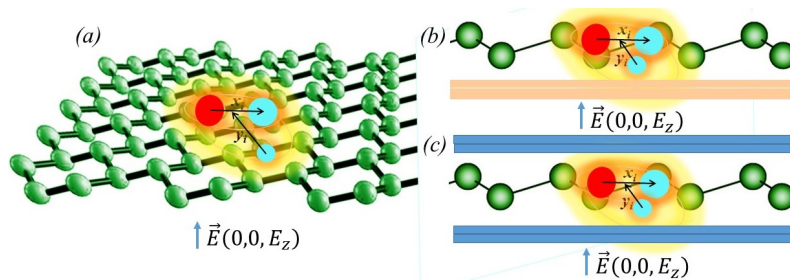


FIG. 2: (Color online) Schematic representation of the X^- trion in the external electric field perpendicular to the Xene layer in (a) freestanding, (b) supported and (c) encapsulated Xenes monolayer. x_i and y_i are Jacobi coordinates for the partition i .

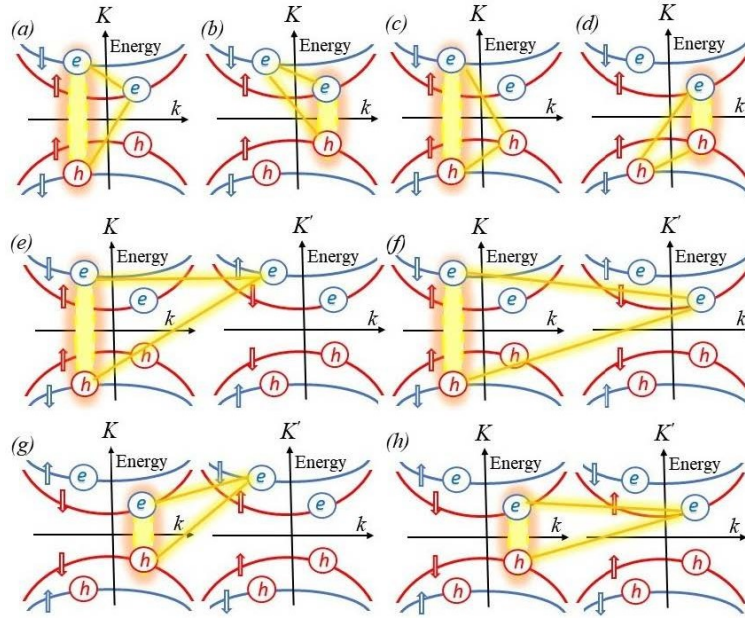


FIG. 3: (Color online) Schematic representation of the low-energy band structure for 2D Xenes material and formation of the intravalley X^- and X^+ trions and intervalley X^- trions. (a) and (b), and (c) and (d) represent the intravalley X^- and X^+ , respectively. (e), (f), (g), and (h) correspond to the intervalley X^- trions with the decrease masses from the biggest (spin-valley configuration (e)) to the smallest one (spin-valley configuration (h)). Intervalley X^+ trions have the same masses as X^- .

TABLE I: Input parameters for calculations of BEs of trions in the freestanding (FS) and encapsulating Xene monolayers. The notations are the following: $2\Delta_{gap}$ is the total gap between conduction and valence bands; d_0 is the buckling parameter; v_F is the Fermi velocity; l is the monolayer thickness; ϵ is the dielectric constant of the Xenes monolayer; ρ_0 is the screening distance; E_c is a critical electric field.

2D material	κ	$2\Delta_{gap}$, meV	d_0 , Å	v_F , $\times 10^5$, m/s	l , nm	ϵ	ρ_0 , nm	E_c , V/Å
FS Si	1	1.9 [96]	0.46 [97]	6.5 [96]	0.4 [43]	11.9	2.38	0.55
FS Ge	1	33 [96]	0.676 [97]	6.2 [96]	0.45	16	4.23	0.3
FS Sn	1	101 [96]	0.85 [96]	5.5 [96]	0.5	24	5.99	0.2
Si (hBN, type I)	4.89	27 [52]	0.46 [52]	4.33 [52]	0.333 [52]	11.9	0.41	none

A excitons and for B excitons. Following *ab initio* calculations [46] which determined that the crystal structure of silicene becomes unstable around 2.6 V/Å, we consider in our calculations electric fields up to 2.7 V/Å and study the formations of trions in Xenes at the range of the external electric field from the critical value up to 2.7 V/Å. Results of calculations of dependencies of trions BE on the external electric field are presented in Fig. 4.

The results of our calculations for the BEs of intravalley trions in a singlet state in freestanding Xenes monolayer are presented in Fig. 4a. The BE increases for all materials as E_\perp increases. In addition, in FS Si, Ge, and Sn, we observe a non-negligible difference in the BE of trions formed by A and B excitons. These differences slightly increase as the electric field increases. The trion BEs for FS Ge and FS Sn are qualitatively similar to FS Si, but they are smaller than freestanding silicene. The curves for FS Ge and Sn qualitatively resemble that of FS silicene, but at 2.7 V/Å FS germanene reaches a maximum trions BE of 24.8 (24.3) meV, and the maximum BE for FS stanene is roughly 21.1 (20.5) meV, significantly smaller than for FS silicene – 30.1 (29.8) meV. In parentheses the BEs of trions formed by B excitons are given. The percent differences between the trion BE of FS Si and FS Ge and FS Si and FS Sn at the largest electric field considered, are 82% (81%) and 70% (69%), respectively.

In Fig. 4b the dependencies of the binding energies for intervalley singlet state trions in spin-valley configurations shown in Figs. 4e and 3h as functions of external electric field are displayed. The corresponding BE are about 2 – 4% larger and qualitatively resemble that of the intravalley trions: i. the increase of the BE as the external electric field increases; ii. BEs for FS silicene, germanene, and stanene are qualitatively similar; iii. a non-negligible difference in the BE of trions formed by A and B excitons.

While the intravalley X^- and X^+ trions must exist in the spin-singlet state, whereas the intervalley trions can exist

in either the singlet or triplet states. In Fig. 4b the dependencies of the binding energies for intervalley $L = 1$ and $S = 3/2$ state trions as functions of the applied external electric field are shown. The BEs of triplet state trions in the FS silicene and germanene monolayers are about three times smaller than that for singlet state trions. Our calculations show unbound triplet state trions in the FS stanene. The decrease of the trion binding energy in the triplet state is due to the centrifugal repulsion.

In Fig. 4d the intravalley trion BEs in Xenes monolayer supported on a SiO_2 and hBN encapsulated are presented. In our calculations, the role of the substrate and the encapsulation by hBN is considered through the potential (6) with $\kappa = (\varepsilon_1 + \varepsilon_2)/2$, where ε_1 and ε_2 are the dielectric constants of two materials that the Xene layer is surrounded by. The comparison of the BEs shows that the FS monolayers exhibit by far the largest BEs, due to the much weaker dielectric screening induced by the environment compared to Xenes supported on the SiO_2 or hBN encapsulated. Hence, the trion BE is the largest for the freestanding Xenes and gets progressively smaller for Xene supported on SiO_2 , and is the smallest for hBN encapsulated. Thus, the trions BE is extremely sensitive to the dielectric environment.

We calculated a probability distribution for three particles that form a trion in the Xene. In Fig. 5 interparticle radial probability distributions for intravalley and intervalley trions in the silicene monolayer are shown. The difference in the probability distribution is related to the difference of the effective masses μ of intravalley and intervalley trions. The probability distribution for the intravalley trion is computed for the spin-valley configuration shown in Fig. 3a and that for the intervalley trions is calculated for the spin-valley configuration in Fig. 3e with the highest mass. The analysis of the dependence of the probability distributions of three particles on the hyperradius ρ and the external electric field leads to the following conclusion: the increase of the external electric field gives the increase of the trions BE and makes trions more compact since the greater binding energy increases the trion formation probability.

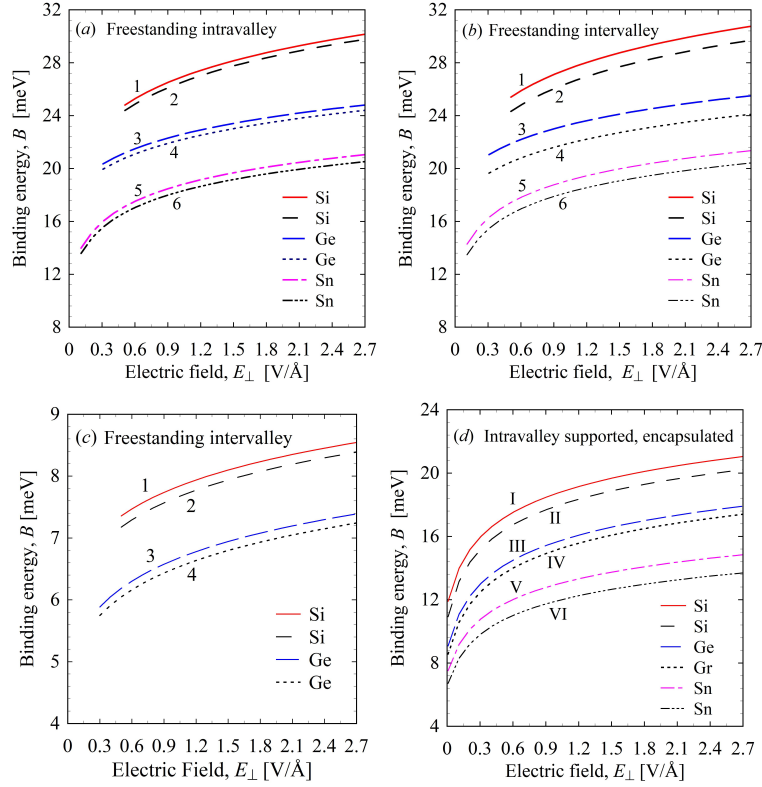


FIG. 4: (Color online) Dependencies of the BE of intravalley and intervalley trions in silicene, germanene, and stanene on the applied electric field. Curves 1, 3, and 5 correspond to the trions formed by A excitons coupling an electron (X^-) or hole (X^+), curves 2, 4, and 6 correspond to the trions formed by B excitons coupling an electron (X^-) or hole (X^+). (a) Freestanding intravalley singlet state trions. (b) Freestanding intervalley singlet state trions. (c) Freestanding intervalley triplet state trions. (d) Intravalley singlet state trions in Xenes monolayer supported on an SiO_2 substrate (curve I, III, and V) and hBN encapsulated (curves II, IV, and VI). The plots for FS Xenes are truncated for the external electric field E_\perp less than a critical field.

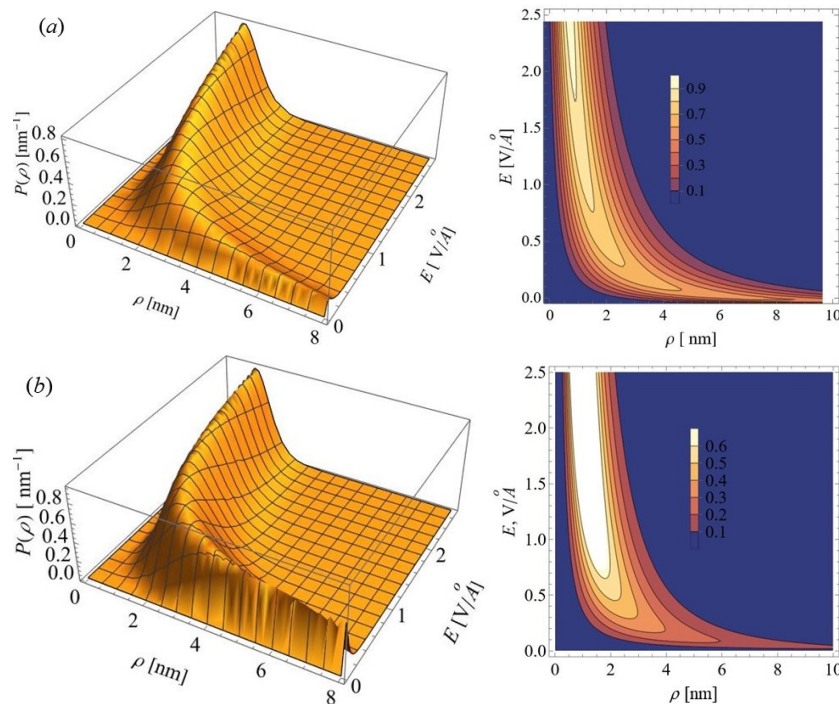


FIG. 5: (Color online) Dependence of the probability distribution of three particles in freestanding silicene on hyperradius ρ and applied electric field for (a) intravalley and (b) intervalley X^- trion.

IV. CONCLUSION

In summary, we predict the existence of electrically-controlled trions in Xenes monolayers. We have applied the hyperspherical harmonics method to the calculation of BEs for the trion and predict formations of trions in freestanding, supported, and encapsulated Xenes in an external electric field perpendicular to monolayers. Results of BEs calculation for trions formed by A and B excitons show a non-negligible differences in trions energies which slightly increase as the electric field increases. The BEs of the intravalley and intervalley trions in the singlet state can be tuned in the range of 24 – 31 meV for silicene, 21 – 26 meV for germanene, and 14 – 20 meV for stanene by varying the external electric field from the critical value that is specific for each material up to 2.7 V/Å. Let us note that the trion binding energy in Xenes are the same order as in TMDC monolayers [38]. The dependence of the BE for the silicene, germanene and stanene as a function of the electric field are qualitatively similar. Our findings pave a way toward manipulating the trion BE by the external electric field.

The maximum BEs of intervalley triplet state trions is about 7.4 meV and 8.5 meV in silicene and germanene, respectively. In stanene the triplet state trions are unbound. To understand the importance of the screened electron-hole interaction in formation of trions in Xenes we computed the BEs for Xenes supported on SiO_2 and hBN encapsulated. It is demonstrated that the dielectric environment has a significant effect on the trion BE by decreasing it.

Results of calculations of the probability distribution show the increase of a compactness of trions with the increase of the electric field, since the greater binding energy increases the trion formation probability.

-
- [1] M. A. Lampert, Mobile and immobile effective-mass-particle complexes in nonmetallic solids, *Phys. Rev. Lett.* **1**, 450 (1958).
 - [2] A. Kormányos, G. Burkard, M. Gmitra, J. Fabian, V. Zólyomi, N. D. Drummond, and V. Fal'ko, $\mathbf{k}\cdot\mathbf{p}$ theory for two-dimensional transition metal dichalcogenide semiconductors, *2D Mater.* **2**, 022001 (2015).
 - [3] G. Wang, A. Chernikov, M. M. Glazov, T. F. Heinz, X. Marie, T. Amand, B. Urbaszek, Excitons in atomically thin transition metal dichalcogenides, *Rev. Mod. Phys.* **90**, 21001 (2018).
 - [4] K. F. Mak, K. He, C. Lee, et al., Tightly bound trion in monolayer MoS_2 , *Nat. Mater.* **12**, 207 (2013).
 - [5] H. Yu, X. Cui, X. Xu, and W. Yao, Valley excitons in two-dimensional semiconductors, *Natl. Sci. Rev.* **2**, 57 (2015).
 - [6] T. C. Berkelbach and D. R. Reichman, Optical and excitonic properties of atomically thin transition-metal dichalcogenides, *Annu. Rev. Condens. Matter Phys.* 2018. **9**, 379–96 (2018).

- [7] M. V. Durnev and M. M. Glazov, Excitons and trions in two-dimensional semiconductors based on transition metal dichalcogenides, *Phys. Usp.* **61**, 825 (2018).
- [8] R. Ya. Kezerashvili, Few-body systems in condensed matter physics, *Few-Body Syst.* **60**, 52 (2019).
- [9] M. A. Semina and R. A. Suris, Localized excitons and trions in semiconductor nanosystems, *Phys. Usp.* **65**, 111 (2022).
- [10] T. C. Berkelbach, M. S. Hybertsen, and D. R. Reichman, Theory of neutral and charged excitons in monolayer transition metal dichalcogenides, *Phys. Rev. B* **88**, 045318 (2013).
- [11] A. Ramirez-Torres, V. Turkowski, and T. S. Rahman, Time-dependent density-matrix functional theory for trion excitations: application to monolayer MoS₂ and other transition-metal dichalcogenides, *Phys. Rev. B* **90**, 085419 (2014).
- [12] M. Z. Mayers, T. C. Berkelbach, M. S. Hybertsen, and D. R. Reichman, Binding energies and spatial structures of small carrier complexes in monolayer transition-metal dichalcogenides via diffusion Monte Carlo, *Phys. Rev. B* **92**, 161404 (2015).
- [13] I. Kylänpää and H.-P. Komsa, H.-P.: Binding energies of exciton complexes in transition metal dichalcogenide monolayers and effect of dielectric environment, *Phys. Rev. B* **92**, 205418 (2015).
- [14] K. A. Velizhanin and A. Saxena, Excitonic effects in 2D semiconductors: path integral Monte Carlo approach, *Phys. Rev. B* **92**, 195305 (2015).
- [15] D. K. Zhang, D. W. Kidd, and K. Varga, Excited biexcitons in transition metal dichalcogenides, *Nano Lett.* **15**, 7002 (2015).
- [16] B. Ganchev, N. Drummond, I. Aleiner, and V. Fal'ko, Three-particle complexes in two-dimensional semiconductors, *Phys. Rev. Lett.* **114**, 107401 (2015).
- [17] D. W. Kidd, D. K. Zhang, and K. Varga, Binding energies and structures of two-dimensional excitonic complexes in transition metal dichalcogenides, *Phys. Rev. B* **93**, 125423 (2016).
- [18] M. Szyniszewski, E. Mostaani, N. D. Drummond, and V. I. Fal'ko, Binding energies of trions and biexcitons in two-dimensional semiconductors from diffusion quantum Monte Carlo calculations, *Phys. Rev. B* **95**, 081301(R) (2017).
- [19] E. Mostaani, M. Szyniszewski, C. H. Price, R. Maezono, M. Danovich, et al., Diffusion quantum Monte Carlo study of excitonic complexes in two-dimensional transition-metal dichalcogenides, *Phys. Rev. B* **96**, 075431 (2017).
- [20] T. Deilmann and K. S. Thygesen, Dark excitations in monolayer transition metal dichalcogenides, *Phys. Rev. B* **96**, 201113(R) (2017).
- [21] R. Ya. Kezerashvili and Sh. M. Tsiklauri, Trion and biexciton in monolayer transition metal dichalcogenides, *Few-Body Syst.* **58**, 18 (2017).
- [22] M. Donck, M. Zarenia, and F. Peeters, Excitons, trions, and biexcitons in transition-metal dichalcogenides: magnetic-field dependence, *Phys. Rev. B* **97**, 195408 (2018).
- [23] L. S. R. Cavalcante, D. R. da Costa, G. A. Farias, D. R. Reichman, and A. Chaves, Stark shift of excitons and trions in two-dimensional materials, *Phys. Rev. B* **98**, 245309 (2018).
- [24] M. Florian, M. Hartmann, A. Steinhoff, et al., The dielectric impact of layer distances on exciton and trion BEs in van der Waals heterostructures, *Nano Lett.* **18**, 2725 (2018).
- [25] I. Filikhin, R. Ya. Kezerashvili, Sh. M. Tsiklauri, and B. Vlahovic, Trions in bulk and monolayer materials: Faddeev equations and hyperspherical harmonics, *Nanotechnology* **29**, 124002 (2018).
- [26] A. Torche and G. Bester, First-principles many-body theory for charged and neutral excitations: trion fine structure splitting in transition metal dichalcogenides, *Phys. Rev. B* **100**, 201403(R) (2019).
- [27] D. V. Tuan, A. M. Jones, M. Yang, X. Xu, and H. Dery, Virtual trions in the photoluminescence of monolayer transition-metal dichalcogenides, *Phys. Rev. Lett.* **122**, 217401 (2019).
- [28] J. Fu, J. M. R. Cruz, and F. Qu, Valley dynamics of different trion species in monolayer WSe₂, *Appl. Phys. Lett.* **115**, 082101 (2019).
- [29] J. Yan and K. Varga, Excited-state trions in two-dimensional materials, *Phys. Rev. B* **101**, 235435 (2020).
- [30] Y. V. Zhumagulov, A. Vagov, D. R. Gulevich, P. E. Faria Junior, and V. Perebeinos, Trion induced photoluminescence of a doped MoS₂ monolayer, *J. Chem. Phys.* **153**, 044132 (2020).
- [31] Y. V. Zhumagulov, A. Vagov, N. Yu. Senkevich, D. R. Gulevich, and V. Perebeinos, Three-particle states and brightening of intervalley excitons in a doped MoS₂ monolayer, *Phys. Rev. B* **101**, 245433 (2020).
- [32] M. Glazov, Optical properties of charged excitons in two-dimensional semiconductors, *J. Chem. Phys.* **153**, 034703 (2020).
- [33] M. Van der Donck, M. Zarenia, and F. M. Peeters, Excitons and trions in monolayer transition metal dichalcogenides: a comparative study between the multiband model and the quadratic single-band model, *Phys. Rev. B* **96**, 035131 (2017).
- [34] Y.-W. Chang and Y.-C. Chang, Variationally optimized orbital approach to trions in two-dimensional materials, *J. Chem. Phys.* **155**, 024110 (2021).
- [35] F. Marsusi, E. Mostaani, and N. D. Drummond, Quantum Monte Carlo study of three-dimensional Coulomb complexes: trions and biexcitons, hydrogen molecules and ions, helium hydride cations, and positronic and muonic complexes, *Phys. Rev. A* **106**, 062822 (2022).
- [36] M. A. Semina, J. V. Mamedov, and M. M. Glazov, Excitons and trions with negative effective masses in two-dimensional semiconductors, *Oxford Open Materials Science*, **3**, itad004 (2023).
- [37] K. Mohseni, M. R. Hadizadeh, T. Frederico, D. R. da Costa, and A. J. Chaves, Trion clustering structure and BE in two-dimensional semiconductor materials: Faddeev equations approach, *Phys. Rev. B* **107**, 165427 (2023).
- [38] R. Ya. Kezerashvili, S. M. Tsiklauri, and A. Dublin, Trions in two-dimensional monolayers within the hyperspherical harmonics method: application to transition metal dichalcogenides, *Phys. Rev. B* **109**, 085406 (2024).
- [39] A. Molle, J. Goldberger, M. Houssa, Y. Xu, S.-C. Zhang, and D. Akinwande, Buckled two-dimensional Xene sheets, *Nat. Mater.* **16**, 163 (2017).
- [40] J. Zheng, Y. Xiang, C. Li, R. Yuan, F. Chi, and Y. Guo, All-optically controlled topological transistor based on Xenex,

Phys. Rev. Appl. **14**, 034027 (2020).

- [41] L. Matthes, O. Pulci, and F. Bechstedt, Massive Dirac quasiparticles in the optical absorbance of graphene, silicene, germanene, and tinene, *J. Phys.: Condens. Matter* **25**, 395305 (2013).
- [42] A. Acun, B. Poelsema, H. J. W. Zandvliet, and R. van Gastel, The instability of silicene on Ag(111), *Appl. Phys. Lett.* **103**, 263119 (2013).
- [43] L. Tao, E. Cinquanta, D. Chiappe, C. Grazianetti, M. Fanciulli, M. Dubey, A. Molle, and D. Akinwande, Silicene field-effect transistors operating at room temperature, *Nat. Nanotechnol.* **10**, 227 (2015).
- [44] B. Aufray, A. Kara, S. Vizzini, H. Oughaddou, C. Léandri, B. Ealet, and G. Le Lay, Graphene-like silicon nanoribbons on Ag(110): A possible formation of silicene, *Appl. Phys. Lett.* **96**, 183102 (2010).
- [45] P. De Padova, C. Quaresima, C. Ottaviani, P. M. Sheverdyaeva, P. Moras, C. Carbone, D. Topwal, B. Olivieri, A. Kara, H. Oughaddou, B. Aufray, and G. Le Lay, Evidence of graphene-like electronic signature in silicene nanoribbons, *Appl. Phys. Lett.* **96**, 261905 (2010).
- [46] N. D. Drummond, V. Zólyomi, and V. I. Fal'ko, Electrically tunable band gap in silicene, *Phys. Rev. B* **85**, 075423 (2012).
- [47] M. Ezawa, Valley-polarized metals and quantum anomalous Hall effect in silicene, *Phys. Rev. Lett.* **109**, 055502 (2012).
- [48] M. E. Dávila, L. Xian, S. Cahangirov, A. Rubio, and G. L. Lay, Germanene: a novel two-dimensional germanium allotrope akin to graphene and silicene, *New J. Phys* **16**, 095002 (2014).
- [49] A. J. Mannix, B. Kiraly, M. C. Hersam, and N. P. Guisinger, Synthesis and chemistry of elemental 2D materials, *Nat. Rev. Chem.* **1**, 0014 (2017).
- [50] C. Grazianetti, C. Martella, and A. Molle, The Xenes generations: a taxonomy of epitaxial single-element 2D materials, *Phys. Status Solidi RRL* **14**, 1900439 (2020).
- [51] D. Di Sante, X. Wu, M. Fink, W. Hanke, and R. Thomale, Triplet superconductivity in the Dirac semimetal germanene on a substrate, *Phys. Rev. B* **99**, 201106 (2019).
- [52] L. Li, X. Wang, X. Zhao, and M. Zhao, Moiré superstructures of silicene on hexagonal boron nitride: A first-principles study, *Phys. Lett. A* **377**, 2628 (2013).
- [53] A. I. Khan, T. Chakraborty, N. Acharjee, and S. Subrina, Stanene-hexagonal boron nitride heterobilayer: structure and characterization of electronic property, *Sci. Rep.* **7**, 16347 (2017).
- [54] S. Saxena, R. P. Chaudhary, and S. Shukla, Stanene: atomically thick free-standing layer of 2D hexagonal tin, *Sci. Rep.* **6**, 31073 (2016).
- [55] M. Ezawa, Quantum Hall effects in silicene, *J. Phys. Soc. Jpn.* **81**, 064705 (2012).
- [56] R. Ya. Kezerashvili and A. Spiridonova, Effects of parallel electric and magnetic fields on Rydberg excitons in buckled two-dimensional materials, *Phys. Rev. B* **103**, 165410 (2021).
- [57] F. Bechstedt, L. Matthes, P. Gori, and O. Pulci, Infrared absorbance of silicene and germanene, *Appl. Phys. Lett.* **100**, 261906 (2012).
- [58] L. Stille, C. J. Tabert, and E. J. Nicol, Optical signatures of the tunable band gap and valley-spin coupling in silicene, *Phys. Rev. B* **86**, 195405 (2012).
- [59] M. Fadaie, N. Shahtahmassebi, and M. R. Roknabad, Effect of external electric field on the electronic structure and optical properties of stanene, *Opt. Quantum Electron.* **48**, 440 (2016).
- [60] D. Muoi, N. N. Hieu, C. V. Nguyen, B. D. Hoi, H. V. Nguyen, N. D. Hien, N. A. Poklonski, S. S. Kubakaddi, and H. V. Phuc, Magneto-optical absorption in silicene and germanene induced by electric and Zeeman fields, *Phys. Rev. B* **101**, 205408 (2020).
- [61] S. Chowdhury and D. Jana, A theoretical review on electronic, magnetic and optical properties of silicene, *Rep. Prog. Phys.* **79**, 126501 (2016).
- [62] X. Zhai, Y.-T. Wang, R. Wen, S.-X. Wang, Y. Tian, X. Zhou, W. Chen, and Z. Yang, Valley-locked thermospin effect in silicene and germanene with asymmetric magnetic field induced by ferromagnetic proximity effect, *Phys. Rev. B* **97**, 085410 (2018).
- [63] M. Ezawa, Valley-polarized metals and quantum anomalous Hall effect in silicene, *Phys. Rev. Lett.* **109**, 055502 (2012).
- [64] A. Zhao and B. Wang, Two-dimensional graphene-like Xenes as potential topological materials, *APL Mater.* **8**, 030701 (2020).
- [65] V. Y. Tsaran and S. G. Sharapov, Landau levels and magnetic oscillations in gapped Dirac materials with intrinsic Rashba interaction, *Phys. Rev. B* **90**, 205417 (2014).
- [66] C.-H. Chen, W.-W. Li, Y.-M. Chang, C.-Y. Lin, S.-H. Yang, Y. Xu, and Y.-F. Lin, Negative-differential-resistance devices achieved by band-structure engineering in silicene under periodic potentials, *Phys. Rev. Appl.* **10**, 044047 (2018).
- [67] J.-K. Lyu, S.-F. Zhang, C.-W. Zhang, and P.-J. Wang, Stanene: a promising material for new electronic and spintronic applications, *Ann. Phys. (Berlin, Ger.)* **531**, 1900017 (2019).
- [68] N. R. Glavin, R. Rao, V. Varshney, E. Bianco, A. Apte, A. Roy, E. Ringe, and P. M. Ajayan, Emerging applications of elemental 2D materials, *Adv. Mater.* **32**, 1904302 (2020).
- [69] C. Grazianetti, C. Martella, and A. Molle, 8 - Two-dimensional Xenes and their device concepts for future micro- and nanoelectronics and energy applications, edited by L. Tao and D. Akinwande, *Micro and Nano Technologies* (Elsevier, 2020), pp. 181-219.
- [70] F. Bechstedt, P. Gori, and O. Pulci, Beyond graphene: clean, hydrogenated and halogenated silicene, germanene, stanene, and plumbene, *Prog. Surf. Sci.* **96**, 100615 (2021).
- [71] C.-C. Liu, W. Feng, and Y. Yao, Quantum spin Hall effect in silicene and two-dimensional germanium, *Phys. Rev. Lett.* **107**, 076802 (2011).
- [72] M. Ezawa, Monolayer topological insulators: silicene, germanene, and stanene, *J. Phys. Soc. Japan* **84**, 121003 (2015).

- [73] L. Matthes, S. Küfner, J. Furthmüller, and F. Bechstedt, Quantization and topological states in the spin Hall conductivity of low-dimensional systems: An ab initio study, *Phys. Rev. B* **93**, 121106 (2016).
- [74] F. Matusalem, D. S. Koda, F. Bechstedt, M. Marques, and L. K. Teles, Deposition of topological silicene, germanene and stanene on graphene-covered sic substrates, *Sci. Rep.* **7**, 15700 (2017).
- [75] X.-L. Yu, L. Huang, and J. Wu, From a normal insulator to a topological insulator in plumbene, *Phys. Rev. B* **95**, 125113 (2017).
- [76] M. N. Brunetti, O. L. Berman, and R. Ya. Kezerashvili, Can freestanding Xene monolayers behave as excitonic insulators?, *Phys. Lett. A* **383**, 482 (2019).
- [77] M. N. Brunetti, O. L. Berman, and R. Ya. Kezerashvili, Optical properties of excitons in buckled two-dimensional materials in an external electric field, *Phys. Rev. B* **98**, 125406 (2018).
- [78] O. Pulci, P. Gori, D. Grassano, M. D'Alessandro, and F. Bechstedt, Transitions in Xenes between excitonic, topological and trivial insulator phases: influence of screening, band dispersion and external electric field, *SciPost Phys.* **15**, 025 (2023).
- [79] N. S. Rytova, Screened potential of a point charge in a thin film, *Proc. MSU Phys., Astron.* **3**, 30 (1967), https://www.researchgate.net/publication/320224883_Screened_potential_of_a_point_charge_in_a_thin_film.
- [80] L. V. Keldysh, Coulomb interaction in thin semiconductor and semimetal films, *JETP Lett.* **29**, 658 (1979).
- [81] C. J. Tabert and E. J. Nicol, Dynamical polarization function, plasmons, and screening in silicene and other buckled honeycomb lattices, *Phys. Rev. B* **89**, 195410 (2014).
- [82] A. H. Castro Neto, F. Guinea, N. M. R. Peres, K. S. Novoselov, and A. K. Geim, The electronic properties of graphene, *Rev. Mod. Phys.* **81**, 109 (2009).
- [83] D. S. L. Abergel, V. Apalkov, J. Berashevich, K. Ziegler, and T. Chakraborty, Properties of graphene: a theoretical perspective, *Adv. Phys.* **59**, 261 (2010).
- [84] M. Ezawa, A topological insulator and helical zero mode in silicene under an inhomogeneous electric field, *New J. Phys.* **14**, 033003 (2012).
- [85] M. Ezawa, Spin-valley optical selection rule and strong circular dichroism in silicene, *Phys. Rev. B* **86**, 161407(R) (2012).
- [86] T. C. Berkelbach, M. S. Hybertsen, and D. R. Reichman, Theory of neutral and charged excitons in monolayer transition metal dichalcogenides, *Phys. Rev. B* **88**, 045318 (2013).
- [87] M. Fogler, L. Butov, and K. Novoselov, High-temperature superfluidity with indirect excitons in van der Waals heterostructures, *Nat. Commun.* **5**, 4555 (2014).
- [88] O. L. Berman and R. Ya. Kezerashvili, High-temperature superfluidity of the two component Bose gas in a transition metal dichalcogenide bilayer, *Phys. Rev. B* **93**, 245410 (2016).
- [89] G. Wang, A. Chernikov, M. M. Glazov, T. F. Heinz, X. Marie, T. Amand, and B. Urbaszek, Colloquium: excitons in atomically thin transition metal dichalcogenides, *Rev. Mod. Phys.* **90**, 021001 (2018).
- [90] O. L. Berman and R. Ya. Kezerashvili, Superfluidity of dipolar excitons in a transition metal dichalcogenide double layer, *Phys. Rev. B* **96**, 094502 (2017).
- [91] P. Cudazzo, I. V. Tokatly, and A. Rubio, Dielectric screening in two-dimensional insulators: implications for excitonic and impurity states in graphane, *Phys. Rev. B* **84**, 085406 (2011).
- [92] J. Avery, *Hyperspherical Harmonics*, Kluwer Academic, Dordrecht, 1989.
- [93] R.I. Jibuti and K. V. Shitikova: *Method of hyperspherical functions in atomic and nuclear physics*, Energoatomizdat, Moscow, 270p. 1993. (in Russian).
- [94] L.D. Faddeev and S.P. Merkuriev, *Quantum scattering theory for several particle systems* (Kluwer Academic, Dordrecht, 1993) pp. 398.
- [95] I. Filikhin, R. Ya. Kezerashvili, and B. Vlahovic, The charge and mass symmetry breaking in the KK \bar{K} system, *J. Phys. G: Nucl. Part. Phys.* **51**, 035102 (2024).
- [96] S. Balendhran, S. Walia, H. Nili, S. Sriram, and M. Bhaskaran, Elemental analogues of graphene: silicene, germanene, stanene, and phosphorene, *Small* **11**, 640 (2015).
- [97] Z. Ni, Q. Liu, K. Tang, J. Zheng, J. Zhou, R. Qin, Z. Gao, D. Yu, and J. Lu, Tunable bandgap in silicene and germanene, *Nano Lett.* **12**, 113 (2012).